# Original Article

# Long intergenic non-protein coding RNA 1949 suppresses rituximab resistance in diffuse large B-cell lymphoma via H3K27me3-mediated ONECUT2 silencing

Shusen Lin, Shenrong Mo, Hongyao Chen, Chengcai Yang, Shikun Wang, Yueyun Xie

Hematology and Oncology Department, No. 924 Hospital of PLA Joint Logistic Support Force, Guilin, Guangxi, China

Received March 19, 2025; Accepted July 24, 2025; Epub September 15, 2025; Published September 30, 2025

Abstract: Objective: To investigate the role of long non-coding RNA LINC01949 in mediating rituximab sensitivity and its underlying epigenetic mechanisms. Methods: Expression of LINC01949 was analyzed in rituximab-sensitive and -resistant diffuse large B-cell lymphoma (DLBCL) cell lines using Gene Expression Omnibus datasets. Functional assays involved LINC01949 knockdown in sensitive cells and overexpression in resistant cells, followed by evaluation of drug response (IC50, apoptosis) and protein levels. Mechanistic studies examined H3K27me3 modification and one cut homeobox 2(ONECUT2) expression. Rescue experiments employed H3K27me3 demethylase inhibitor (GSK-J4) and ONECUT2 inhibitor (CSRM617). EZH2 binding to LINC01949 was assessed by RIP-qPCR. Results: LINC01949 expression was significantly downregulated in rituximab-resistant cells. Its knockdown in sensitive cells conferred resistance, while overexpression in resistant cells restored sensitivity. Mechanistically, LINC01949 loss reduced H3K27me3 levels, leading to derepression of the oncogenic transcription factor ONECUT2. Pharmacological restoration of H3K27me3 or inhibition of ONECUT2 reversed resistance. RIP-qPCR confirmed direct binding of LINC01949 to EZH2, which was diminished in resistant cells. Conclusion: LINC01949 suppresses rituximab resistance in DLBCL by promoting H3K27me3-dependent silencing of ONECUT2. These findings highlight the LINC01949-H3K27me3-ONECUT2 axis as a key epigenetic pathway and suggest potential targets to overcome resistance in DLBCL.

**Keywords:** Long intergenic non-protein coding RNA 1949, one cut homeobox 2, H3K27me3, diffuse large B-cell lymphoma

## Introduction

Diffuse large B-cell lymphoma (DLBCL), accounting for approximately 30% of all non-Hodgkin lymphomas [1], is the most common and aggressive subtype. The R-CHOP regimen comprising rituximab, cyclophosphamide, doxorubicin, vincristine, and prednisone - has been the frontline therapy for over two decades, with rituximab, an anti-CD20 monoclonal antibody, serving as its key component [2, 3]. However, 30-40% of patients exhibit primary resistance or relapse after treatment. Even advanced therapies such as CD19-targeted CAR T-cell therapy eventually encounter acquired resistance. This highlights the urgent need to elucidate the molecular mechanisms underpinning immune and chemoresistance to

enable the development of precision treatment strategies.

Long non-coding RNAs (IncRNAs) are RNA transcripts longer than 200 nucleotides, transcribed by RNA polymerase II and lacking open reading frames [4]. They regulate gene expression through interactions with DNA, RNA, and proteins at epigenetic, transcriptional, and post-transcriptional levels, and have been implicated in tumor progression and therapy resistance [5]. LINC01949, a 2898-bp IncRNA located on chromosome 5, has not been studied in cancer. Bioinformatic analysis of the GSE159852 dataset suggests its involvement in rituximab resistance in DLBCL [6].

One cut homeobox 2(ONECUT2), a member of the One Cut transcription factor family [7], mod-

Table 1. The sequences of primers

LINIO04040 Feet and	E' 0040404400044004044004 0'
LINC01949-Forward	5'-CCACAGAAGGCAAGCAGAAGCA-3'
LINC01949-Reverse	5'-CAGGCACCCAAGGGAATCTCCT-3'
ONECUT2-Forward	5'-CGCAGGATGTGGAAGTGGCTTC-3'
ONECUT2-Reverse	5'-TGTTCGGCGTTGGAGGTCAGT-3'
GAPDH-Forward	5'-CACCCACTCCTCCACCTTTGAC-3'
GAPDH-Reverse	5'-GTCCACCACCCTGTTGCTGTAG-3'

ulates gene expression by binding specific DNA sequences. Its aberrant expression promotes cancer stemness and chemoresistance by activating the WNT/β-catenin pathway and inducing epithelial-mesenchymal transition (EMT) [8-11]. H3K27me3, a repressive histone mark catalyzed by the PRC2 complex, typically silences oncogenes through chromatin compaction. However, in DLBCL, CpG hypermethylation at the ONECUT2 promoter [12, 13] and potential antagonism between DNA methylation and H3K27me3 suggest loss of H3K27me3 at this site, possibly enabling ONECUT2 derepression. Nonetheless, direct evidence of H3K27me3 alterations at the ONECUT2 locus and their link to rituximab resistance is lacking. In this study, we re-analyzed data from the GSE159852 dataset, compared rituximab-sensitive and -resistant DLBCL cell lines, and explored how LINCO1949 regulates ONECUT2 expression to promote rituximab resistance.

# Materials and methods

Differentially expressed IncRNA analysis and mapping

Differential expression analysis of IncRNAs in the GSE159852 dataset was performed using GEO2R. Significantly dysregulated transcripts were identified using thresholds of [log2FC] > 0.1 and adjusted P < 0.05, and visualized with volcano plots. Raw sequencing data were processed through a transcriptome analysis pipeline: reads were aligned to the GRCh38 genome using HISAT2, transcripts were assembled with StringTie, and differentially expressed mRNAs were identified and visualized via mRNA-specific volcano plots. Gene Ontology (GO) enrichment analysis was conducted using GOSeq. topGO, and HMMscan, with significant terms (P < 0.05) illustrated using Directed Acyclic Graphs (DAGs) to represent functional hierarchies.

Cell culture and transfection

Rituximab-sensitive SU-DHL-4 and rituximab-resistant SU-DHL-8 cell lines (MesenCTCC) were cultured in RPMI-1640 medium supplemented with 10% fetal bovine serum and 1% penicillin/streptomycin at 37°C in a 5%  $\rm CO_2$  incubator. Transfections were carried out using Lipe2000

(GZYXbio, Guangzhou) according to the manufacturer's instructions. The overexpression plasmid, negative control siRNA (5'-TTCTCC-GAACGTGTCACGT-3'), and LINCO1949 siRNA (targeting NR\_130914.1, positions 2479-2501; 5'-AAGCTTCATTAGCAAAGAAGA-3') were synthesized by Ige Biotechnology Co., Ltd. (Guangzhou).

qPCR detection of LINC01949 and ONECUT2 expression

Following treatment, cells were collected by trypsinization and centrifugation. Total RNA was extracted using RNAiso Plus reagent (RN6501, Aidlab, Beijing) according to the manufacturer's protocol. RNA was precipitated with isopropanol, washed three times with 75% ethanol, air-dried, and dissolved in RNase-free water. Reverse transcription was performed using 1 µg of RNA with the PrimeScript™ RT Master Mix (RR036A, Takara, Japan). Quantitative PCR was conducted using 2x UniTag SYBR qPCR Master Mix (P1504, TIANGEN Biotech, Guangzhou) on a QuantStudio 6 Flex Real-Time PCR System with gene-specific primers (All-perfect Biological Technology Co., Ltd.). Primer sequences are shown in **Table 1**.

Flow cytometric detection of apoptosis

After treatment, cells were resuspended and centrifuged at  $300\times g$  for 5 minutes, then washed three times with ice-cold PBS. Apoptosis was assessed using the Annexin V-FITC/PI Apoptosis Detection Kit (MA0220, Dalian Meilun Biotechnology Co., Ltd., China) following the manufacturer's instructions. Cells were resuspended in 1× binding buffer at 1 ×  $10^6$  cells/mL, incubated with 2  $\mu$ L Annexin V-FITC and 2  $\mu$ L propidium iodide for 10 minutes in the dark. Samples were analyzed using a BD Accuri<sup>TM</sup> C6 flow cytometer, and data were processed with NovoExpress software.

CCK-8 assay for half-maximal inhibitory concentration (IC50) determination

Cells were seeded in 96-well plates at a density of 5,000 cells per well. After 48 hours of drug treatment or transfection, the medium was removed, and cells were washed three times with PBS. Then, 10  $\mu L$  of CCK-8 reagent (CKO4, Dojindo, Japan) and 90  $\mu L$  of complete medium were added to each well and incubated at 37°C with 5% CO $_2$  for 30 minutes. Absorbance at 450 nm was measured using an ELx800 microplate reader (BioTek, USA). The IC50 values were calculated using a four-parameter logistic regression model.

Western blot for target protein expression

After treatment, cells were lysed using RIPA buffer (P0013B, Beyotime) supplemented with 10 µM GSK-J4 (G10347, Psaitong). Protein concentrations were determined using the BCA Protein Assay Kit. Equal amounts of protein (50 µg per lane) were separated by 10% SDS-PAGE and transferred to PVDF membranes (ISE000010, Millipore). Membranes were blocked with 3% BSA (ST023, Beyotime) for 1 hour and incubated overnight at 4°C with primary antibodies: anti-ONECUT2 (1:2000, DF13779, Affinity), anti-H3K27me3 (1:2000, DF6941, Affinity), anti-β-actin (1:1000, ab6276, Abcam), and anti-BCL2 (1:1000, ab32124, Abcam). After washing, membranes were incubated with HRP-conjugated secondary antibodies (1:5000, ab205718, Abcam) for 2 hours. Protein bands were visualized using ECL reagents and quantified with ImagePro Plus 6.0 software, using β-actin as a loading control. All experiments were performed in triplicate.

Quantitative assessment of EZH2 binding to LINCO1949 via RIP-qPCR

Approximately  $1 \times 10^7$  SU-DHL-8 and SU-DHL-4 cells were collected, washed with ice-cold PBS, and cross-linked with 1% formaldehyde in PBS for 10 minutes at room temperature. The reaction was quenched with glycine, and cells were pelleted by centrifugation (1500 g, 4°C, 5 minutes). Cells were lysed in RIPA buffer (P0013B, Beyotime Biotechnology, Shanghai) with protease and RNase inhibitors on ice for 15 minutes, vortexing every 5 minutes, followed by centrifugation at 14,000 g (10 minutes, 4°C). Supernatants were collected, and

50 µL were saved as input controls. Protein A/G magnetic beads were washed and incubated with 5 µg of anti-EZH2 antibody (ab191250, Abcam) or an IgG isotype control for 1 hour at room temperature. After preparing the antibody-bead complex, 100 µL of cell lysate was added and the mixture was rotated overnight at 4°C. Washes were performed with Low-salt, High-salt, and LiCl buffers. RNA extraction was performed, and purified RNA was dissolved in 20 µL of RNase-free water. The LINC01949 content input and RIP samples were analyzed by qPCR, and the enrichment fold was calculated using the ΔΔCt method. The Imprint® RNA Immunoprecipitation Kit was obtained from Sigma-Aldrich (Merck, Germany).

Statistical analysis

IBM SPSS Statistics 26.0 was used for data analysis. Each experiment was repeated independently three times. The experimental results were statistically analyzed using one-way ANOVA followed by the LSD test. A *P* value < 0.05 was considered statistically significant.

# Results

Differences in transcriptomes of cell lines with different sensitivity to rituximab

We performed differential expression analysis of IncRNAs in DLBCL cell lines with distinct rituximab sensitivities using the GSE159852 dataset. Volcano plot visualization identified LINC01949 as the most significantly dysregulated IncRNA (Figure 1A). qPCR validation confirmed that the expression of LINC01949 in rituximab-resistant SU-DHL-8 cells was 60.33 ± 10.97% of that in rituximab-sensitive SU-DHL-4 cells (P < 0.01, Figure 1B), indicating significant downregulation of LINC01949 in resistant cells. To further characterize transcriptional alterations, we analyzed mRNA profiles using the HISAT2, StringTie, and Ballgown pipelines on the same dataset. A total of 1,539 differentially expressed mRNAs were identified, with 611 upregulated and 928 downregulated in resistant cells compared to sensitive counterparts (Figure 1C). Gene Ontology (GO) enrichment analysis using GOSeq, topGO, and HMMscan revealed three major functional clusters: biological processes were predominantly enriched in cell differentiation; cellular com-

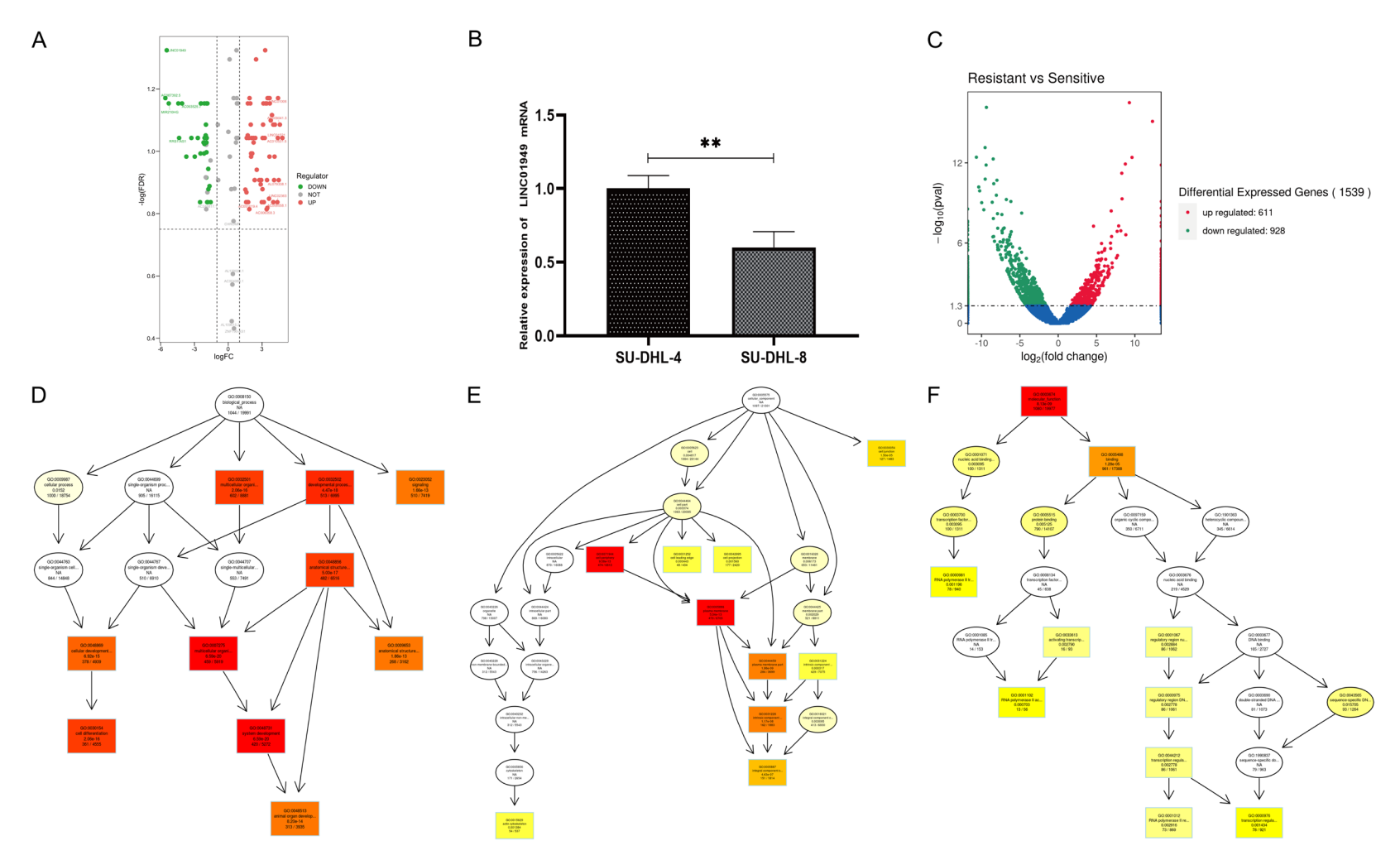


Figure 1. Differences in the transcriptomes of cell lines with different sensitivity to rituximab. A: Expression differences in the non-coding transcriptome between rituximab-resistant and sensitive cell lines, with LINCO1949 showing the most significant difference, displayed in volcano plots. B: qPCR confirmation of the differential expression of LINCO1949 in SU-DHL-4 and SU-DHL-8 cell lines, \*\*P < 0.01. C: Differential expression of mRNA transcriptomes in rituximab-resistant and sensitive cell lines, shown in volcano plots. D-F: GO analysis of differentially expressed genes and enrichment results for MF, BP, and CC in Directed Acyclic Graph format.

ponents were significantly associated with the actin cytoskeleton and integral plasma membrane structures; and molecular functions were strongly linked to RNA polymerase II regulatory region DNA binding and transcription regulatory region sequence-specific DNA binding (**Figure 1D-F**).

LINC01949 regulates rituximab resistance in DLBCL cell lines

To investigate the relationship between LINC-01949 expression and rituximab resistance in DLBCL cell lines, we manipulated LINC01949 expression in two cell lines. SU-DHL-4 and SU-DHL-8. Specifically, we inhibited LINC01949 expression in SU-DHL-4 and increased its expression in SU-DHL-8 (Figure 2A and 2B). After these adjustments, we assessed rituximab resistance in both cell lines. CCK-8 assay results showed that decreased LINC01949 expression in SU-DHL-4 cells led to increased rituximab resistance, marked by a significant increase in IC50 (Figure 2C). Conversely, in SU-DHL-8, increased LINC01949 expression was associated with decreased rituximab resistance, reflected by a significant decrease in IC50 (Figure 2D). Flow cytometry analysis revealed that, at the same rituximab concentration, reduced LINC01949 expression in SU-DHL-4 cells resulted in significantly lower apoptosis (Figure 2E). In contrast, increased LINC01949 expression in SU-DHL-8 cells led to a significant rise in apoptotic cell proportion (Figure 2F).

LINC01949 affects ONECUT2 expression by regulating histone H3K27me3 methylation levels

Intersection analysis of significantly enriched gene sets from GO analysis revealed that the gene encoding ONECUT2 was the only gene concurrently present in gene sets associated with cell differentiation, actin cytoskeleton organization, and RNA polymerase II regulatory region DNA binding (Figure 3A). ONECUT2, a member of the ONECUT transcription factor family, is known to promote tumor cell stemness and facilitate EMT, contributing to chemotherapy resistance. We investigated whether LINCO1949 correlates with ONECUT2 expression. Western blot analysis showed that elevat-

ed LINC01949 expression led to significant downregulation of ONECUT2 protein levels in both SU-DHL-4 and SU-DHL-8 cell lines, while reduced LINC01949 expression correlated with increased ONECUT2 expression (Figure 3B. 3C). Given previous reports of altered CpG island methylation at the ONECUT2 locus in DLBCL and the mutual exclusivity between DNA methylation and H3K27me3 modifications, we quantified H3K27me3 levels. Western blotting revealed significantly higher basal H3K27me3 modification levels in SU-DHL-4 compared to SU-DHL-8 (Figure 3D). Modulation of LINC01949 expression substantially affected this epigenetic mark: LINC01949 overexpression in SU-DHL-8 significantly elevated H3K27me3 levels (P < 0.01), while LINC01949 knockdown in SU-DHL-4 significantly reduced H3K27me3 levels (P < 0.01), indicating that LINC01949 promotes H3K27me3 modification in DLBCL cell lines (Figure 3E, 3F). To confirm whether LINC01949 regulates ONECUT2 through H3K27me3-mediated silencing, we performed rescue experiments in SU-DHL-4 cells. Upon LINC01949 knockdown, we observed decreased H3K27me3 levels and increased ONECUT2 expression; however, concurrent administration of GSK-J4 (an inhibitor of H3K27me3 demethylation) maintained H3-K27me3 levels and abolished ONECUT2 upregulation despite LINC01949 depletion (Figure 3G). Further functional validation in SU-DHL-4 cells, where LINC01949 knockdown enhances rituximab resistance, revealed that co-treatment with the ONECUT2 inhibitor CSRM617 during LINC01949 knockdown significantly restored apoptosis sensitivity (Figure 3H), confirming that LINC01949 regulates rituximab resistance through ONECUT2. Mechanistically, since H3K27me3 is catalyzed by Polycomb Repressive Complex 2 (PRC2), which includes the core methyltransferase subunits EZH2/ EZH1, we hypothesized that LINC01949 might recruit PRC2 to the ONECUT2 locus. RNA immunoprecipitation (RIP) assays confirmed that LINC01949 directly binds to EZH2 protein in both cell lines, with significantly lower levels of LINC01949-EZH2 complexes detected in SU-DHL-8 cells. This was consistent with their reduced LINC01949 expression and diminished PRC2 recruitment to ONECUT2, resulting in enhanced transcriptional activity of ONECUT2 and increased drug resistance (Figure 3I).

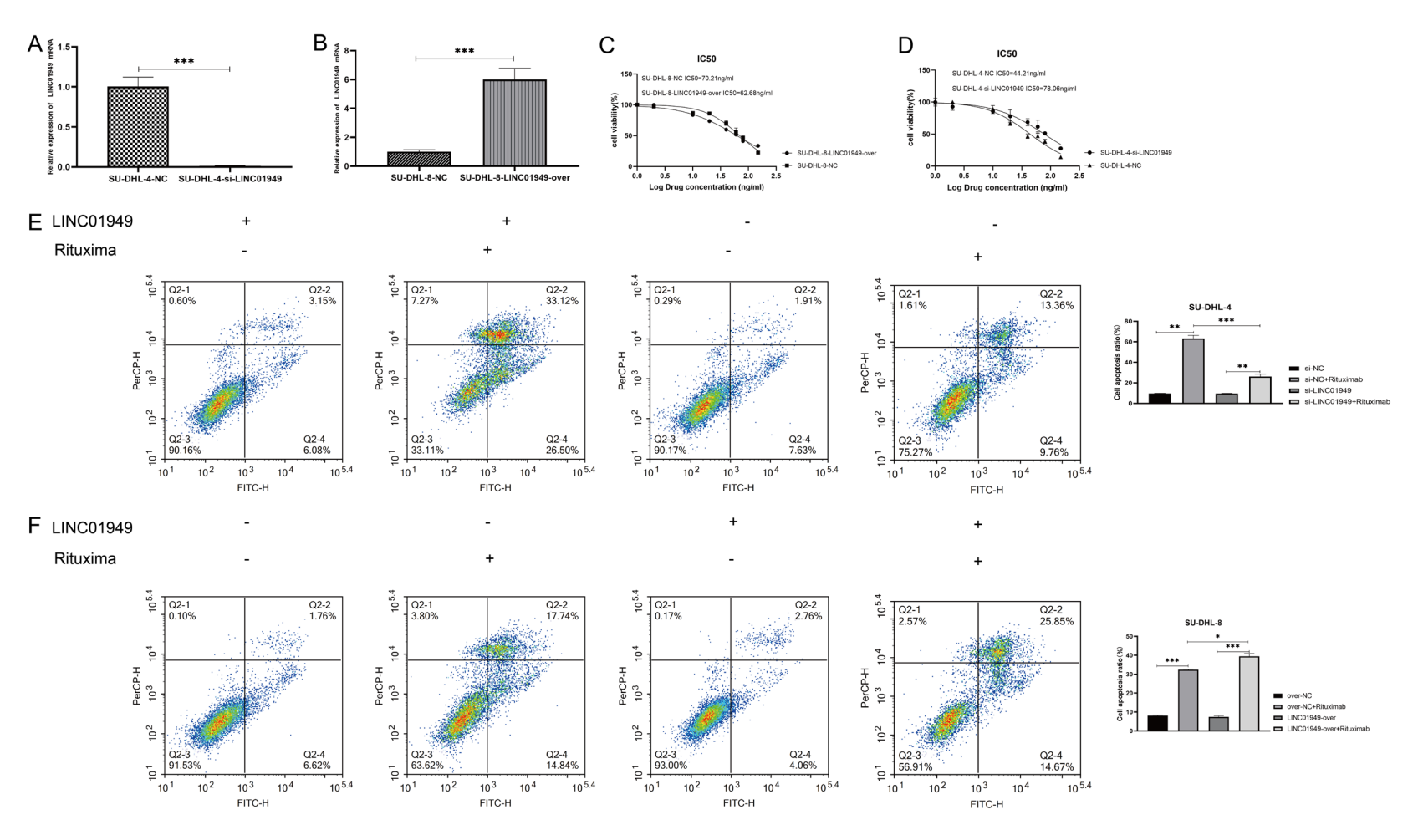


Figure 2. LINC01949 regulates rituximab resistance in DLBCL cell lines. A: qPCR confirmation of siRNA effectiveness. After siRNA transfection, LINC01949 mRNA expression was significantly reduced, \*\*\*P < 0.001. B: qPCR confirmation of the LINC01949 overexpression plasmid effectiveness. After plasmid transfection, LINC01949 mRNA expression significantly increased, \*\*\*P < 0.001. C: CCK-8 assay testing the lethality of different concentrations of rituximab on SU-DHL-4. As LINC01949 expression decreased, SU-DHL-4 showed increased resistance to rituximab. D: CCK-8 assay testing the lethality of different concentrations of rituximab on SU-DHL-8. As LINC01949 expression increased, SU-DHL-8 showed reduced resistance to rituximab. E: Flow cytometry detection of apoptosis levels in SU-DHL-4. Rituximab increased apoptosis, and reducing LINC01949 expression protected SU-DHL-4 from rituximab-induced apoptosis, \*\*P < 0.01, \*\*\*P < 0.001. F: Flow cytometry detection of apoptosis levels in SU-DHL-8. Rituximab increased apoptosis, and enhancing LINC01949 expression promoted rituximab-induced apoptosis, \*P < 0.05, \*\*\*P < 0.001.

# Drug resistance in diffuse large B-cell lymphoma

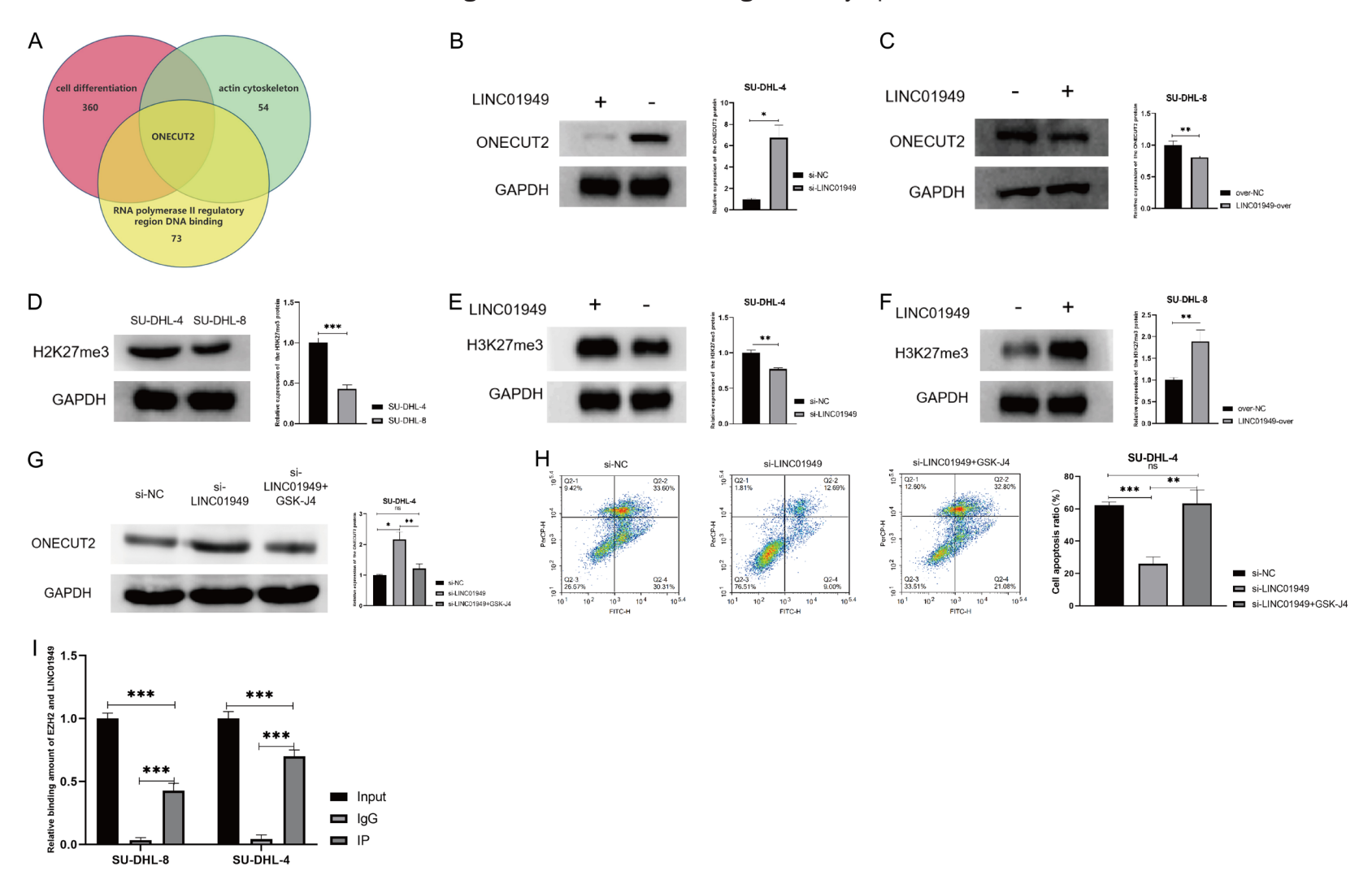


Figure 3. LINCO1949 affects ONECUT2 expression by regulating histone H3K27me3 methylation levels. A: ONECUT2 identified by intersection of three functional subsets in G0 analysis. B, C: Western blot analysis detecting ONECUT2 expression changes under different LINCO1949 expression levels. Increased LINCO1949 expression significantly reduced ONECUT2 protein levels in SU-DHL-4 and SU-DHL-8, \*P < 0.05, \*\*P < 0.01. D: Western blot analysis of H3K27me3 modification levels in SU-DHL-4 and SU-DHL-4 and SU-DHL-8 under different LINCO1949 expression levels. Increased LINCO1949 expression significantly elevated H3K27me3 modification levels in both cell lines, \*\*P < 0.01. G: Western blot analysis in SU-DHL-4 detecting changes in H3K27me3 levels. Reducing LINCO1949 expression significantly reduced ONECUT2 levels, but maintaining H3K27me3 with GSK-J4 prevented changes in H3K27me3 and blocked ONECUT2 upregulation despite LINCO1949 knockdown, ns: P > 0.05, \*P < 0.05, \*P < 0.01. H: Flow cytometry detection of apoptosis levels. Reducing LINCO1949 expression inhibited rituximab-induced apoptosis, \*\*P < 0.001. I: RIP assays validating the binding capacity between the EZH2 protein and LINCO1949. Binding was detected in both SU-DHL-4 and SU-DHL-8, \*\*\*P < 0.001.

# Discussion

Although rituximab effectively prolongs the survival of DLBCL patients, its efficacy can be compromised by acquired or inherent chemotherapy resistance, even when combined with drugs such as cyclophosphamide, doxorubicin, vincristine, and prednisone as part of the standard immunochemotherapy regimen [14]. Understanding the mechanisms underlying rituximab resistance is crucial for developing improved therapies for DLBCL patients. Kauppinen et al. performed high-throughput sequencing on DLBCL cell lines with varying rituximab sensitivities and found differences in their IncRNA transcriptomes [6]. We utilized the GEO2R online analysis tool to analyze and map the sequencing results, identifying LINC01949 as a significantly differentially expressed IncRNA. LINC01949, located at 5q14.3, is a non-coding gene that has not been extensively studied. In this study, we confirmed for the first time the differential expression of LINC01949 in rituximab-resistant DLBCL cell lines and demonstrated that it acts as a tumor suppressor gene. Overexpression of LINC01949 reduced rituximab resistance in DLBCL cells, decreasing the IC50 value of rituximab and enhancing its cytotoxic effect.

Further analysis of the sequencing data revealed differences in the mRNA transcriptomes of DLBCL cell lines with varying rituximab sensitivities. GO analysis of differentially expressed mRNAs showed that the biological processes were mainly related to cell differentiation. Cellular components were predominantly associated with the actin cytoskeleton and the plasma membrane, while molecular functions were enriched in RNA polymerase II regulatory region DNA binding and transcription regulatory region sequence-specific DNA binding [15]. These findings suggest a potential mechanism for drug resistance: the regulation of specific gene promoter regions, leading to altered transcriptional expression levels, which ultimately influence cell proliferation, differentiation, and epithelial-to-mesenchymal transition, contributing to rituximab resistance. By analyzing significant gene sets from GO analysis, we identified ONECUT2 as a key gene associated with drug resistance in DLBCL. ONECUT2, a member of the ONECUT transcription factor family, is involved in regulating proteins related to cell proliferation, migration, adhesion, differentiation, and metabolism [16, 17]. ONECUT2 has been shown to drive castration-resistant prostate cancer [18] and promote lymph node metastasis in colorectal cancer [19, 20]. Our study further demonstrated that LINCO1949 regulates rituximab resistance through ONECUT2 by modulating histone H3K27me3 levels. When LINCO1949 regulation was blocked, rituximab resistance in cells could not be reversed.

While our findings elucidate a novel LINC01949-H3K27me3-ONECUT2 axis in rituximab resistance in DLBCL, several limitations warrant consideration. First, the study primarily relies on in vitro models (SU-DHL-4/SU-DHL-8 cell lines), and the physiological relevance of these findings requires validation in in vivo systems, such as patient-derived xenografts or genetically engineered mouse models. Second, clinical correlations between LINC01949 expression, H3K27me3 levels, ONECUT2 activity, and patient outcomes (e.g., progression-free survival) remain unexplored. Future studies should analyze primary DLBCL samples stratified by treatment response to establish translational relevance. Third, the mechanistic focus on ONECUT2 as the sole effector may overlook additional LINC01949-regulated targets. Genome-wide ChIP-seq or CUT&Tag profiling under LINC01949 modulation could identify broader epigenetic networks. Lastly, although pharmacological inhibition (GSK-J4, CSRM617) rescued phenotypic effects, the therapeutic feasibility of targeting this axis in vivo - particularly regarding toxicity and specificity - requires systematic evaluation. Future work should prioritize developing LINC01949-mimetic oligonucleotides or ONECUT2 degraders and testing their efficacy in combination with rituximab to overcome clinical resistance.

In conclusion, our transcriptome analysis of rituximab-sensitive and -resistant cells revealed significant differential expression of LINCO1949 and ONECUT2. We further confirmed that LINCO1949 modulates ONECUT2 expression by regulating H3K27me3 levels, ultimately impacting rituximab resistance in DLBCL.

# Acknowledgements

We thank the No. 924 Hospital of PLA Joint Logistic Support Force for supporting this study.

# Disclosure of conflict of interest

None.

Address correspondence to: Yueyun Xie, Hematology and Oncology Department, No. 924 Hospital of PLA Joint Logistic Support Force, No. 1 Xinqiao Yuan Road, Guilin, Guangxi, China. Tel: +86-0773-2081685; E-mail: xieyueyun181@163.com

### References

- [1] Shi Y, Xu Y, Shen H, Jin J, Tong H and Xie W. Advances in biology, diagnosis and treatment of DLBCL. Ann Hematol 2024; 103: 3315-3334.
- [2] Coiffier B, Lepage E, Briere J, Herbrecht R, Tilly H, Bouabdallah R, Morel P, Van Den Neste E, Salles G, Gaulard P, Reyes F, Lederlin P and Gisselbrecht C. CHOP chemotherapy plus rituximab compared with CHOP alone in elderly patients with diffuse large-B-cell lymphoma. N Engl J Med 2002; 346: 235-242.
- [3] Pfreundschuh M, Kuhnt E, Trümper L, Osterborg A, Trneny M, Shepherd L, Gill DS, Walewski J, Pettengell R, Jaeger U, Zinzani PL, Shpilberg O, Kvaloy S, de Nully Brown P, Stahel R, Milpied N, López-Guillermo A, Poeschel V, Grass S, Loeffler M and Murawski N; MabThera International Trial (MInT) Group. CHOPlike chemotherapy with or without rituximab in young patients with good-prognosis diffuse large-B-cell lymphoma: 6-year results of an open-label randomised study of the MabThera International Trial (MInT) Group. Lancet Oncol 2011; 12: 1013-1022.
- [4] Bridges MC, Daulagala AC and Kourtidis A. LNCcation: IncRNA localization and function. J Cell Biol 2021; 220: e202009045.
- [5] Zhang J, Zhu H, Li L, Gao Y, Yu B, Ma G, Jin X and Sun Y. New mechanism of LncRNA: in addition to act as a ceRNA. Noncoding RNA Res 2024; 9: 1050-1060.
- [6] Karstensen KT, Schein A, Petri A, Bøgsted M, Dybkær K, Uchida S and Kauppinen S. Long non-coding RNAs in diffuse large B-cell lymphoma. Noncoding RNA 2020; 7: 1.
- [7] Yu J, Li D and Jiang H. Emerging role of ONECUT2 in tumors. Oncol Lett 2020; 20: 328.
- [8] Lin M, Tu RH, Wu SZ, Zhong Q, Weng K, Wu YK, Lin GT, Wang JB, Zheng CH, Xie JW, Lin JX, Chen QY, Huang CM, Cao LL and Li P. Increased ONECUT2 induced by Helicobacter pylori promotes gastric cancer cell stemness via an AKTrelated pathway. Cell Death Dis 2024; 15: 497.
- [9] Zhang L, Li C, Song X, Guo R, Zhao W, Liu C, Chen X, Song Q, Wu B and Deng N. Targeting ONECUT2 inhibits tumor angiogenesis via down-regulating ZKSCAN3/VEGFA. Biochem Pharmacol 2024; 225: 116315.

- [10] Shen M, Dong C, Ruan X, Yan W, Cao M, Pizzo D, Wu X, Yang L, Liu L, Ren X and Wang SE. Chemotherapy-induced extracellular vesicle miRNAs promote breast cancer stemness by targeting ONECUT2. Cancer Res 2019; 79: 3608-3621.
- [11] Hu J, Chen Y, Li X, Miao H, Li R, Chen D and Wen Z. THUMPD3-AS1 is correlated with non-small cell lung cancer and regulates self-renewal through miR-543 and ONECUT2. Onco Targets Ther 2019; 12: 9849-9860.
- [12] Seo EH, Kim HJ, Kim JH, Lim B, Park JL, Kim SY, Lee SI, Jeong HY, Song KS and Kim YS. ONECUT2 upregulation is associated with CpG hypomethylation at promoter-proximal DNA in gastric cancer and triggers ACSL5. Int J Cancer 2020; 146: 3354-3368.
- [13] Pike BL, Greiner TC, Wang X, Weisenburger DD, Hsu YH, Renaud G, Wolfsberg TG, Kim M, Weisenberger DJ, Siegmund KD, Ye W, Groshen S, Mehrian-Shai R, Delabie J, Chan WC, Laird PW and Hacia JG. DNA methylation profiles in diffuse large B-cell lymphoma and their relationship to gene expression status. Leukemia 2008; 22: 1035-1043.
- [14] Zhang J, Gu Y and Chen B. Drug-resistance mechanism and new targeted drugs and treatments of relapse and refractory DLBCL. Cancer Manag Res 2023; 15: 245-255.
- [15] Duttke SH, Guzman C, Chang M, Delos Santos NP, McDonald BR, Xie J, Carlin AF, Heinz S and Benner C. Position-dependent function of human sequence-specific transcription factors. Nature 2024; 631: 891-898.
- [16] Leyva-Díaz E. CUT homeobox genes: transcriptional regulation of neuronal specification and beyond. Front Cell Neurosci 2023; 17: 1233830.
- [17] Nepveu A. Role of the multifunctional CDP/ Cut/Cux homeodomain transcription factor in regulating differentiation, cell growth and development. Gene 2001; 270: 1-15.
- [18] Wang Z, Zhao Y, An Z and Li W. Molecular links between angiogenesis and neuroendocrine phenotypes in prostate cancer progression. Front Oncol 2019; 9: 1491.
- [19] Jiang Z, Tai Q, Xie X, Hou Z, Liu W, Yu Z, Liang Z and Chen S. EIF4A3-induced circ\_0084615 contributes to the progression of colorectal cancer via miR-599/ONECUT2 pathway. J Exp Clin Cancer Res 2021; 40: 227.
- [20] Ma T, Qiao T, Huang R, Wang M, Hu H, Yuan Z, Zhu Y, Wu H and Zou X. Long noncoding XLOC\_006390 regulates the proliferation and metastasis of human colorectal cancer via miR-296/ONECUT2 axis. J Oncol 2022; 2022: 4897201.